E-20-K63
#1

Final Report

Development of Innovative SMA Connections and Dampers For Frame Structures Under Extreme Loads

Reginald DesRoches
School of Civil & Environmental Engineering
Atlanta, GA 30332-0355

1.0 Overview

The report below describes the results of Phase I study of SMAs, including testing of SMA bars and Analysis of braced systems using SMAs.

2.0 Experimental Testing of Superelastic NiTi

2.1 25.4 mm (1.0 inch) Diameter Superelastic NiTi Bars

Five 25.4 mm (1.0 inch) diameter superelastic NiTi bars were tested for this part of the study. The bar specimens were machined from an original 31.75 mm (1.25 inch) diameter bar. The overall length of the specimens was 267 mm (10.5 inches) with a reduced diameter length of 127 mm (5.0 inches). The ends of the bar specimens were threaded in order to assist gripping of the large diameter specimens. All specifications for the test specimens were obtained based on the ASTM E8-03 standard for tensile testing of metallic materials. A picture of the machined specimen can be seen in Figure 1. All of the specimens were obtained by hot rolling, straightening, and centerless grinding the same larger diameter specimen in order to ensure the same composition throughout the set given the sensitivity of the material properties of NiTi to the composition of the material. Each specimen had a near-equiatomic composition of 55.95 Wt. % Ni with a balancing Wt. % of Ti. After machining, all of the bars were annealed at 300°C (572°F) for 1.5 hours and immediately water quenched in order to ensure good superelastic behavior. All specimens were previously untested and underwent no mechanical or thermal training before being tested

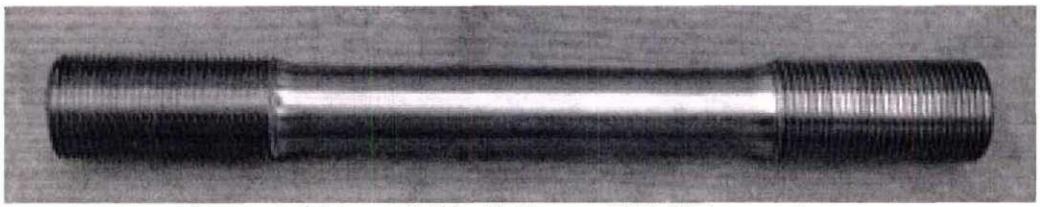

Figure 1. 25.4 mm (1.0 inch) diameter NiTi SE bar specimen

2.2 Test Setup and Loading Protocol

A 2.7 MN (600 kip) MTS uniaxial servo-controlled hydraulic frame was used to test all five of the 25.4 mm (1.0 inch) diameter SE specimens. In order to grip the specimens, the ends of the bars were threaded and screwed into large high strength steel cylinders which were accepted by the hydraulic grips attached to the test frame. An INSTRON 8500 Plus controller was used to apply all loading protocols. The tension only specimens were run in strain control. Because of the occurrence of buckling, the compression specimens were only run up to the 1% strain cycle in strain control in order to calibrate the strain level with the crosshead displacement. The following cycles were then run in displacement control with the strains being measured based on the calibration factor and the crosshead displacement. A similar procedure was used during the testing of the tension-compression specimen. Labview software was used to collect the force from the load cell attached to the testing frame, crosshead displacement, and the strain from the extensometer. The extensometer had a gage length of 101.6 mm (4 inches) as specified by ASTM standards.

Three different loading protocols were implemented in order to accurately simulate strain levels and strain rates experienced by structural members during an earthquake. All of the loading protocols were created to simulate a far field type earthquake. The first loading protocol simulated a tension only loading consisting of increasing strain cycles of 0.5%, 1.0%-4% by increments of 1%, and several cycles at 5% strain. The second loading protocol consisted of compression only cycles to the same strain levels where the SE bar was allowed to undergo buckling during cycling. Two tension only and two compression only tests were run. In both cases, the first test was run quasi-statically at a loading rate of 0.025 Hz and the second test was run dynamically at 1.0 Hz and 1.3 mm/sec (0.05 inch/sec) for the tension only and compression only tests, respectively. A third loading protocol was also implemented which consisted of tension and compression cycles to the same strain levels as specified for the other two loading protocols. The tension-compression test was only run quasi-statically. The three loading protocols can be seen in Figure 2.

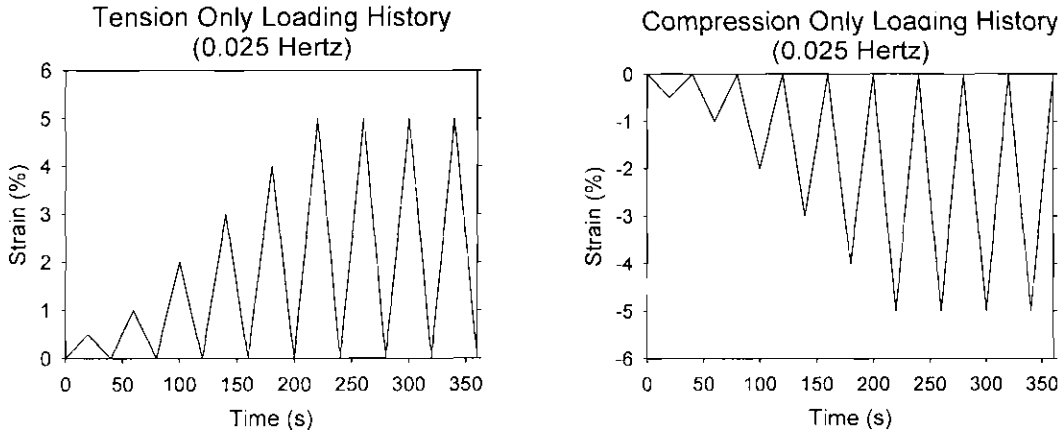

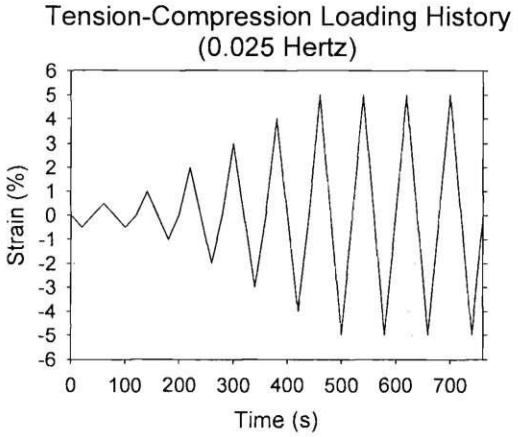

Figure 2. Typical quasi-static loading protocol for the cyclic testing of the 25.4 mm (1.0 inch) diameter SE bars

The performance of the 25.4 mm (1.0 inch) diameter SE bars undergoing the cyclic loadings is evaluated based on the residual strain (ε_R), the forward and reverse transformation stress (σ_L and σ_{UL}), the initial elastic modulus (E_i), and the equivalent viscous damping associated with a given cycle (ξ_{eq}). The residual strain refers to the strain at zero stress at the end of a given cycle and provides a measure of the recentering capability of the material which is particularly important for seismic applications. The forward transformation stress is the stress at which the material begins the detwinning process from the parent austenite phase to the stress-induced martensite phase. The reverse transformation stress is the stress along the unloading curve at which point the material begins to revert back to its original austenite phase. The initial elastic modulus provides a measure of the slope of the initial loading curve before the forward transformation stress is reached. Equivalent viscous damping is a common value used in earthquake engineering to measure the energy dissipation provided by a material or structure by normalizing the energy dissipated with respect to the stiffness of the material.

2.3 Results for the 25.4 mm (1.0 inch) Diameter SE Bars

Tension Only Test Results

The stress-strain plots for both the quasi-static (0.025 Hz) and dynamic (1.0 Hz) tension only tests are presented in Figure 3. The results show good superelastic behavior for the specimens cycled at both loading rates with the formation of a clear loading plateau and the typical flag shape hysteresis associated with NiTi shape memory alloys. Both specimens experienced a brittle failure within the threads before reaching the end of the loading protocol. The quasi-static specimen was only able to undergo a single 5% strain cycle while the dynamic specimen failed on the fourth 5% strain cycle. The failure can most likely be attributed to surface defects in the material as a result of the threading process and suggests that further work needs to be undertaken in order to determine the most adequate way to connect large diameter shape memory alloys to structural systems. Although for both cases, the specimens showed good shape recovery with residual strain remaining below 0.75% for the first 5% strain cycle suggesting that large diameter bars can provide recentering capabilities when deformed to high strain levels.

The quasi-static specimen has a slightly lower loading plateau stress as compared to the dynamic specimen. The loading plateau stresses for the first 5% strain cycle are approximately 441 MPa (64 ksi) and 462 MPa (67 ksi) for the quasi-static and dynamic specimens, respectively. For the dynamically tested bar, there was a significant decrease in the loading plateau stress with continued cycling at the 5% strain level from 462 MPa (67 ksi) for the first 5% strain cycle to 375 MPa (54 ksi) for the last 5% strain cycle. This decrease can be attributed to the formation of permanent slip which tends to assist the forward transformation process. There also appears to be a slight increase in the unloading plateau stress for the dynamic specimen, although to a lesser extent than seen in past studies of smaller diameter specimens. These increases can be attributed to a self-heating of the bar during dynamic cycling due to the exothermic-endothermic process undergone during the phase transformation. During dynamic cycling, the generated heat does not have time to dissipate causing an increase in the loading and unloading plateau stress. The initial elastic modulus was approximately 41 GPa (6000 ksi) for the quasi-static specimen and increased to approximately 47.5 GPa (6900 ksi) for the dynamic specimen. Both specimens show good hysteretic behavior with maximum equivalent viscous damping values of 3.75% and 4.14% for the quasi-static specimen and the dynamic specimen, respectively. The results suggest the large diameter SE NiTi SMAs can be used in tension only bracing systems to provide recentering and some supplemental damping capacity.

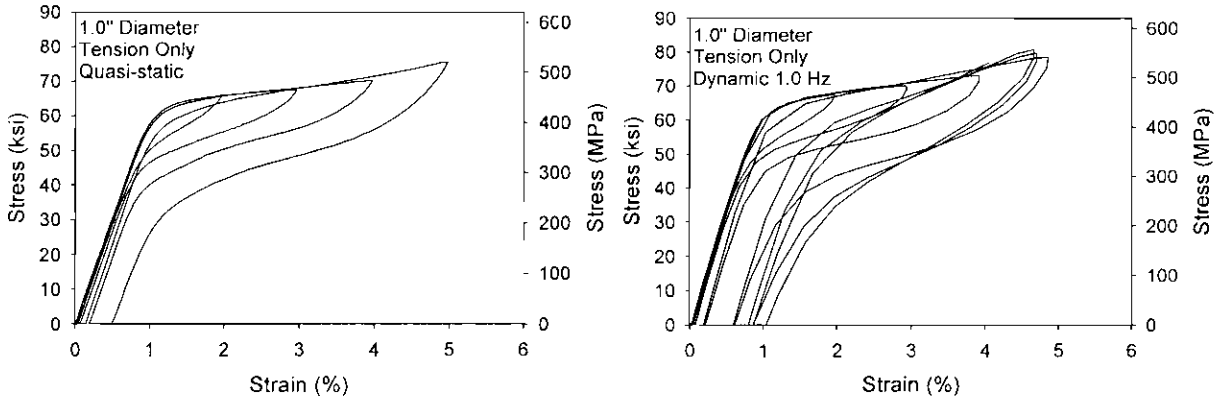

Figure 3. Stress-strain plot for 25.4 mm (1.0 inch) diameter bar tested in tension only both quasi-statically and dynamically

Compression Only Test Results

Figure 4 provides the stress-strain curves for the SE NiTi 25.4 mm (1.0 inch) diameter bar specimens tested quasi-statically (0.025 Hz) and dynamically (1.3 mm/sec (0.05 inch/sec)) under the compression loading protocol previously presented. The results show clear superelastic behavior for the strain cycles up to 2% strain in compression. For higher strain cycles, the specimens underwent significant buckling which resulted in permanent deformation of the material. As with the tensile specimens, the compression specimens failed due to fracture of the specimen at the threads. Figure 5 shows the failed dynamic compression specimens with initiation of the failure at the threads. A clear flag shape hysteresis can be distinguished in the low strain level cycles before the onset of buckling with little residual strain resulting. This result suggest that buckling constrained braces can provide recentering and energy dissipation in both tension and compression.

For the 1% strain cycle, the loading plateau stresses for the quasi-static and dynamic specimens were approximately -604 MPa (-88 ksi) and -641 MPa (-93 ksi), respectively. The loading plateau stress for SMAs in compression is higher than that when the specimens are cycled in tension. This can be attributed to a different deformation mode in compression as opposed to tension. No significant trend in the loading plateau was obtained during continued cycling due to the onset of a buckling deformation mode for higher strain cycles. The initial elastic modulus for both the quasi-static and dynamic specimens showed little difference with values typically around 68 GPa (9900 ksi) for the low level strain cycles. After buckling, the initial elastic modulus decreased significantly due to a softening of the bar. Because of the onset of buckling, equivalent viscous damping values were significantly higher for the compression specimens. The maximum equivalent viscous damping values were 5.71% and 9.58% for the quasi-static specimen and the dynamic specimen, respectively. The larger values for the dynamic specimen can be attributed to the higher strain levels reached before failure. The compression results suggest that SE SMAs can provide good superelastic behavior, particularly if the bars are restrained from buckling.

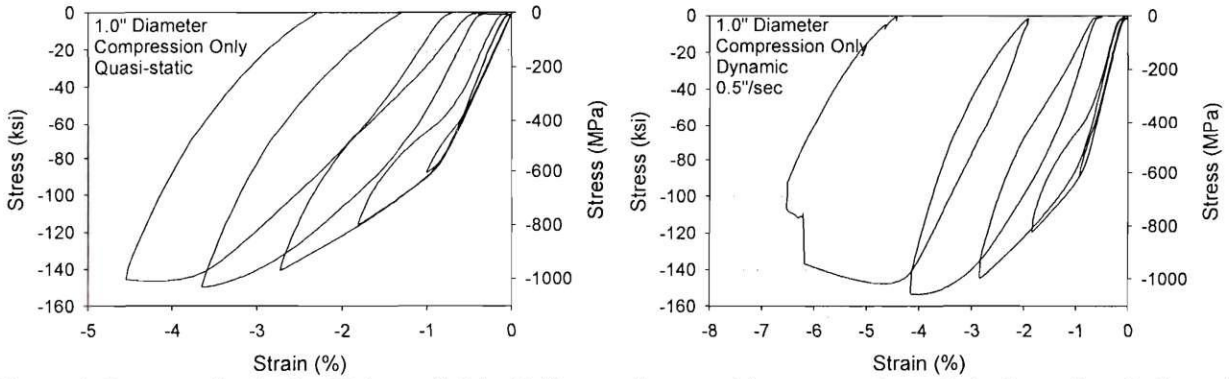

Figure 4. Stress-strain plot for 25.4 mm (1.0 inch) diameter bar tested in compression only both quasi-statically and dynamically

Figure 5. Point of fracture of the compression only specimen tested dynamically at a loading rate of 1.3 mm/sec (0.05 inch/sec)

Tension-Compression Test Results

The stress-strain curve for the 25.4 mm (1.0 inch) diameter SE bar cycled in both tension and compression is shown in Figure 6. The stress-strain curve shows good superelastic behavior in both tension and compression. During testing, the specimen failed at the threads during the 4%

strain cycle in tension. The specimen showed good recentering even during both tension and compression cycling with the maximum residual strains being -0.20% and -0.38% after the 3% strain cycle. The slightly higher residual strain value in compression can be associated with the onset of buckling. The stress-strain curve confirms the results from the tension only and compression only tests and shows that similar behavior can be obtained from specimens cycled in both tension and compression.

The loading plateau stress is significantly higher when the bar is cycled in compression as compared to tension with values equivalent to those found in the previous tests with differences between the loading plateau in tension and compression as high as 241 MPa (35 ksi) for a given cycle. The specimens were also approximately 13.8 GPa (2000 ksi) stiffer in compression than in tension resulting in higher initial elastic modulus values in compression than in tension. This difference needs to be accounted for in future modeling of SE SMA specimens used in building systems for seismic mitigation. The equivalent viscous damping increased from 3.0% to 5.0% going from the 3% strain tension cycle to the 3% strain compression cycle. Overall, the equivalent viscous damping value remains too low to use large diameter SE NiTi SMAs for purely damping applications, although when used in both tension and compression they can provide a moderate amount of supplemental damping to a building system while also providing the recentering capability.

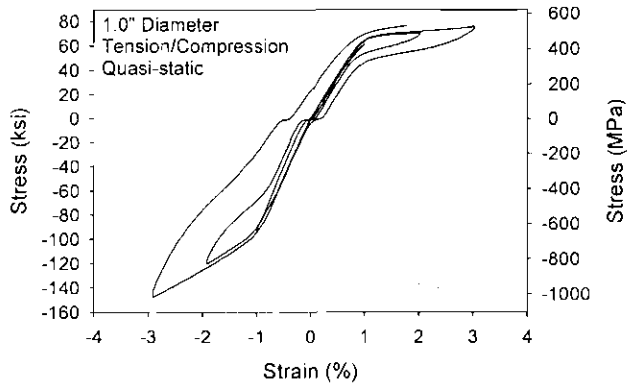

Figure 6. Stress-strain plot for 25.4 mm (1.0 inch) diameter bar tested quasi-statically in both tension and compression

Cyclic Properties of the 25.4 mm (1.0 inch) Diameter SE Bar

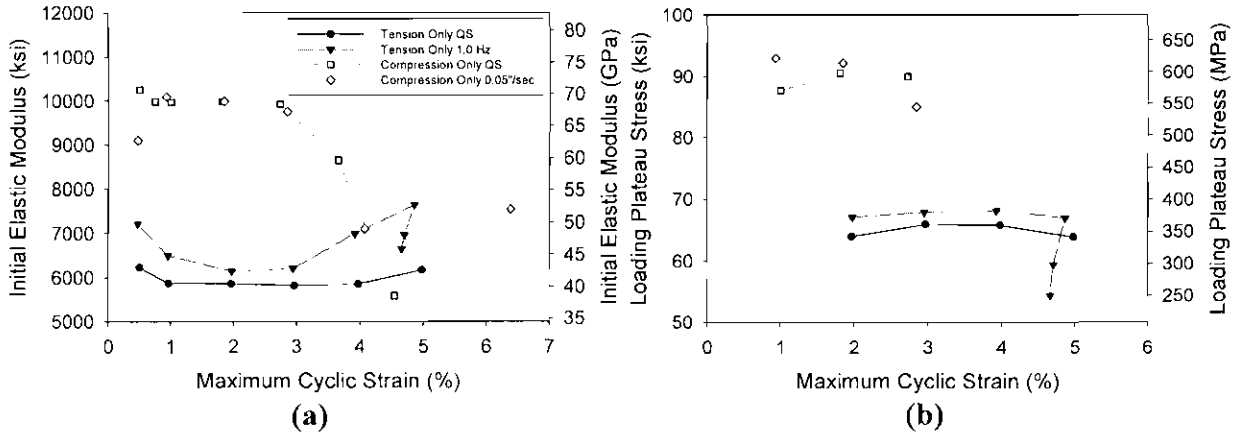

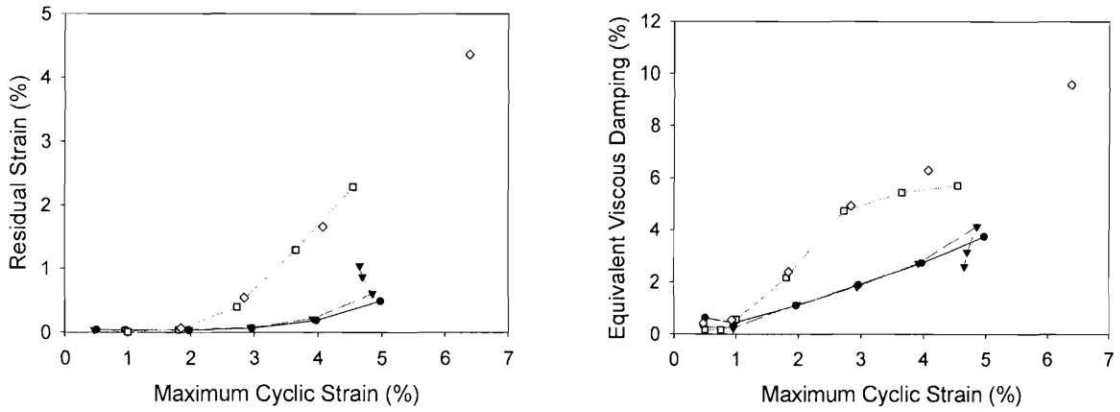

Figure 7. Comparison of SE 25.4 mm (1.0 inch) diameter bars subjected to quasi-static and dynamic cyclic loading in either tension or compression showing: (a) initial elastic modulus, (b) loading plateau stress, (c) residual strain, and (d) equivalent viscous damping

The plots shown in Figure 7 provide the initial elastic modulus, loading plateau stress, residual strain, and equivalent viscous damping values with respect to the maximum cyclic strain for the 25.4 mm (1.0 inch) diameter SE NiTi specimens tested both quasi-statically and dynamically in tension only and compression only. All of the compression only values are presented as absolute values to provide a means of comparing them with the tension only results. Figure 7(a) shows that the compression specimens had a much higher initial elastic modulus as compared to the tension specimens. Although for both the tension and compression specimens, the initial elastic modulus remained constant for low level strain cycles while increasing for higher tensile cycles and decreasing for higher compression cycles. The decrease in the compression cycles is due to a softening of the specimen due to buckling. The difference between the tension and compression values is approximately 28 GPa (4100 ksi) for the 2% strain cycles. No strain rate effect can be seen with the compression specimens while the increased loading rate resulted in an increase in the initial elastic modulus for the tensile specimen.

The variation of loading plateau stress with increased maximum cyclic strain can be seen in Figure 7(b). The loading plateau increases by approximately 172 MPa (25 ksi) when cycled in compression as compared to the loading plateau when cycled in tension to 3% strain. As was previously mentioned, this is due to a different deformation process in compression than in tension. Both the tension and compression specimens showed fairly constant and stable loading plateau stress values until buckling occurred in compression and several cycles at 5% strain in tension which resulted in the formation of permanent slip. Loading rate affected both the compression and tension specimens similarly by increasing the loading plateau stress with an increase in loading rate. The increase was approximately 22 MPa (6.9 ksi) for the tension specimen and 37 MPa (5.3 ksi) for the compression specimen for the 2% strain cycle. Since this strain rate effect is minimal and fairly constant for the tensile specimen, the results suggest that large diameter SE SMAs can perform well under loading rates typical of an earthquake.

Figure 7(c) shows the effect that loading rate has on the residual strain with increased maximum cyclic strain in both tension and compression. For all specimens, the residual strain values remained minimal during the low strain cycles. The compression specimens showed a much larger increase in residual strain to 1.29% and 1.66%, as opposed to the tension specimens,

0.19% and 0.87%, for the 4% strain cycle. This difference can be attributed to permanent deformation due to buckling of the compression specimens during the large strain cycles. The tensile specimens showed good recentering capability even during straining up to 5%. The residual strain results do not show any significant strain rate effects when tested in either compression or tension. The residual strain results prove the suitability of SE SMAs to be used as recentering devices in seismic applications.

Figure 7(d) provides the variation in equivalent viscous damping with respect to maximum cyclic strain and loading rate for both the tension and compression specimens. The specimens cycled in compression provide much higher energy dissipation with equivalent viscous damping values of 5.45% and 6.30% for the 4% strain cycle as opposed to 2.73% equivalent viscous damping obtained for both tension specimens for the 4% strain cycles. The increase equivalent viscous damping can be attributed to the larger hysteresis area associated with the compression specimens due to both the increased loading plateau stress and the onset of buckling resulting in a degradation of the recentering capability in compression. Both the tension and compression specimens do follow the same trend of increasing equivalent viscous damping with increased maximum cyclic strain. As with the other properties, loading rate has very little effect on the equivalent viscous damping value. It is important to note that the equivalent viscous damping values for the SE bars remain fairly low suggesting that they cannot be used for purely damping purposes in seismic applications.

2.4 Midsize (12.7 mm (0.5 inch) and 7.1 mm (0.28 inch)) Superelastic NiTi Bars

12.7 mm (0.5 inch) and 7.1 mm (0.28 inch) diameter SE NiTi bars are tested in this segment of the study in order to evaluate the mechanical behavior of midsize SE bars and to determine if they have similar potential for use in seismic applications as the larger diameter specimens previously presented. All of the specimens had an overall length of approximately 152 mm (6.0 inches) with a reduced length to the specified diameter of 57 mm (2.25 inches). The composition of the 7.1 mm (0.28 inch) diameter bars was 56 Wt. % Ni and 44 Wt. % Ti while the composition for the 12.7 mm (0.5 inch) diameter bars was 55.9 Wt. % Ni and 44.1 Wt. % Ti. The smaller diameter specimens were hot rolled during processing while the larger diameter midsize bars were 30% cold drawn in order to obtain the desired diameter. After machining, all bars were annealed at 350°C (662°F) for 1 hour and then immediately water quenched in order to ensure good superelastic properties. No specimen underwent mechanical or thermal cycling before being tested.

2.5 Test Setup and Loading Protocol

For the midsize specimens, a 250 kN (55 kip) MTS uniaxial servo-controlled hydraulic frame was used to perform all tensile tests. The testing frame was fitted with hydraulic wedge grips which allowed for direct gripping of the specimens and eliminated the need to thread the ends of the specimens. The loading protocol was input using an MTS Testar controller with the cycles being run in strain control based on the output of a 25.4 mm (1.0 inch) gage extensometer in order to ensure proper strain levels were met. Load and displacement measurements were obtained from the internal load cell and crosshead displacement.

The midsize bars underwent a similar tensile loading protocol as the 25.4 mm (1.0 inch) diameter SE bars mentioned previously. The loading protocol was once again developed to simulate the loading of a typical far field type earthquake and consisted of increasing strain cycles of 0.5%, 1.0%-5.0% by increments of 1%, and four 6% strain cycles. Figure 8 provides the typical loading protocol for a specimen cycled quasi-statically. For both sizes of specimens, a quasi-static loading rate (0.025 Hz) was used and dynamic loading rates of 0.5 Hz and 1.0 Hz in order to evaluate the behavior under dynamic loadings typical of an earthquake. As with the larger diameter SE specimens, the performance of the midsize SE specimens was evaluated based on the residual strain, loading plateau stress, unloading plateau stress, and equivalent viscous damping values.

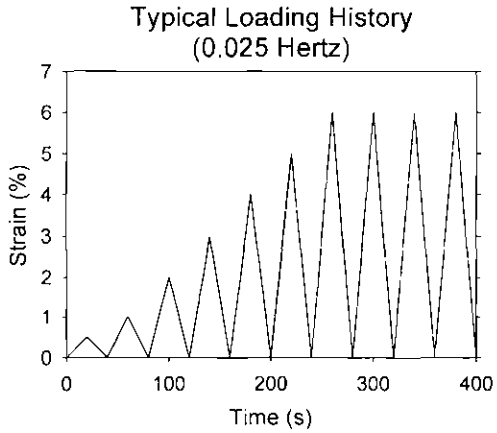

Figure 8. Typical quasi-static loading protocol for the cyclic testing of the midsize SE bars

2.6 Results for Midsize SE Bars

Quasi-static Test Results

The stress-strain plots for the 7.1 mm (0.28 inch) diameter and 12.7 mm (0.5 inch) diameter SE NiTi specimens cycled quasi-statically are presented in Figure 9. There are slight differences in the shape of the stress-strain curves which may be a result of the different processing procedures (hot worked vs. cold drawn). The stress-strain curve for the 7.1 mm (0.28 inch) diameter specimen has a more defined loading and unloading plateau while the plateaus for the 12.7 mm (0.5 inch) specimen is sloped and not as easily distinguished. Although, both specimens do show the flag-shape hysteresis and recentering capability typically associated with superelastic SMAs. Comparing the recentering capability of the two specimens, the residual strain after the first 6% strain cycle was approximately 0.32% and 0.17% for the 7.1 mm (0.28 inch) and 12.7 mm (0.5 inch) bar specimens, respectively. The residual strain values suggest good recentering capabilities even out to large strain levels.

The loading plateau stresses for both the smaller and larger bar specimen were similar. The smaller midsize bar specimen has a forward transformation stress of approximately 345 MPa (50 ksi) and the larger midsize bar specimen has a slightly lower forward transformation stress of 331 MPa (48 ksi). Even though the hysteresis may have different shapes, the stress needed to

induce the martensitic phase transformation does not significantly change. A more significant difference can be seen in the unloading plateau stress which can clearly be defined for the 7.1 mm (0.28 inch) diameter bar, but needs to be estimate based on the inflection point along the unloading curve for the 12.7 mm (0.5 inch) diameter bar. This results in a difference in the equivalent viscous damping values due to the decreased hysteretic area for the larger diameter midsize bar. The equivalent viscous damping for the first 6% strain cycle was approximately 3.87% and 2.12% for the 7.1 mm (0.28 inch) and 12.7 mm (0.5 inch) diameter SE bars, respectively.

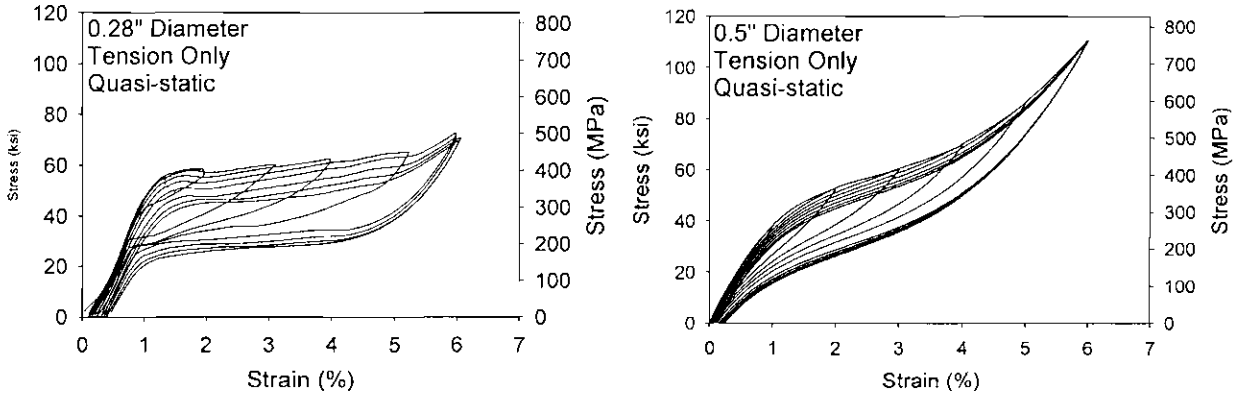

Figure 9. Stress-strain plot for the (a) 7.1 mm (0.28 inch) diameter and (b) 12.7 mm (0.5 inch) diameter SE bars tested in tension at a quasi-static (0.025 Hz) loading rate

Dynamic Test Results

Figure 10 provides the stress-strain curves for the 7.1 mm (0.28 inch) diameter SE specimen cycled dynamically at loading rates of 0.5 Hz and 1.0 Hz. The typical flag shape hysteresis remains even with the dynamic loading rates, but there is an increase in the loading plateau stress and unloading plateau stress with the increased strain rate. The loading plateau stress increases from 345 MPa (50 ksi) for the quasi-static loading to approximately 407 MPa (59 ksi) for both of the dynamic loadings at the first 6% strain cycle. A more significant increase is found in the unloading plateau stress resulting in significant narrowing of the hysteresis. This increase can be associated with a significant self-heating of the specimen and the thermoelastic nature of the material. The narrowing of the hysteresis results in a decrease in the equivalent viscous damping to 2.39% and 1.82% during the first 6% strain cycle for the 0.5 Hz and 1.0 Hz tests, respectively. The decrease in equivalent viscous damping with increased strain rate further suggests that midsize SE SMAs are better suited for recentering devices. The residual strain decreases with increased strain rate to 0.26% and 0.2% for the first 6% strain cycle for the 0.5 Hz and 1.0 Hz test providing better recentering capability at larger strain rates.

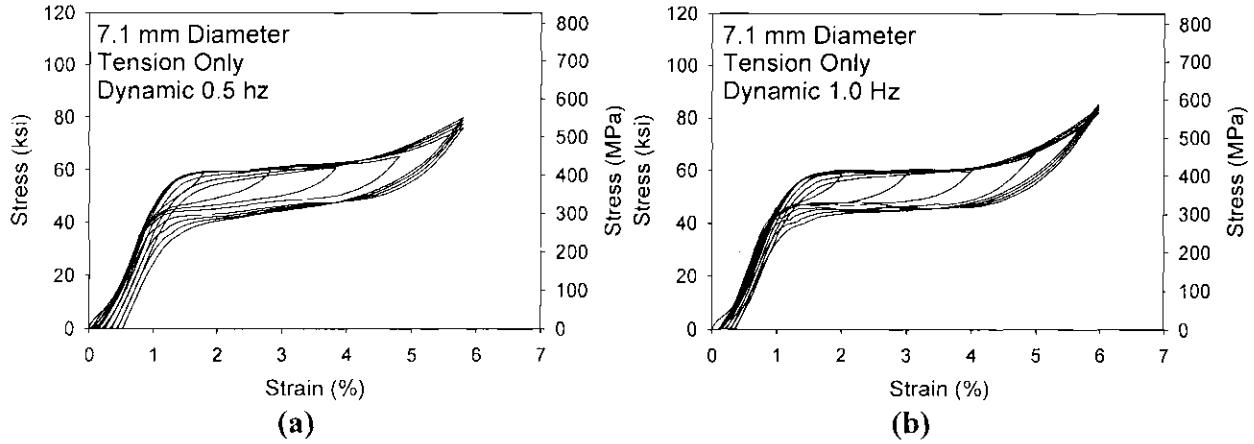

Figure 10. Stress-strain plot for the 7.1 mm (0.28 inch) diameter SE bars tested dynamically in tension at loading rates of (a) 0.5 Hz and (b) 1.0 Hz)

The stress-strain curves for the 12.7 mm (0.5 inch) diameter specimens cycled dynamically are shown in Figure 11. As with the smaller specimens, the 12.7 mm (0.5 inch) diameter specimens show good superelastic behavior with a flag shape hysteresis and good recentering capability. The loading plateau stress increased with the increased loading rate from 331 MPa (48 ksi) when cycled quasi-statically to approximately 414 MPa (60 ksi) when cycled dynamically for the first 6% strain cycle. A larger increase also occurred in the unloading plateau stress resulting in the same narrowing of the hysteresis and reduction of the energy dissipation capacity of the specimens at higher strain levels. The equivalent viscous damping values were 1.83% and 1.72% for the 0.5 Hz and 1.0 Hz specimens, respectively, for the first 6% strain cycle, which was a decrease from the 2.12% equivalent viscous damping value obtained for the specimen cycled quasi-statically. These equivalent viscous damping values were also less than those obtained for the 7.1 mm (0.28 inch) diameter specimens. The residual strain after the first 6% strain cycle showed little change at the different loading rates with values of 0.17%, 0.15%, and 0.16% for the quasi-static, dynamic 0.5 Hz, and dynamic 1.0 Hz tests, respectively. The results further suggest the capability of using midsize diameter bars for seismic and earthquake engineering applications and the results compare favorably with the trends found during the 25.4 mm (1.0 inch) diameter SE specimens.

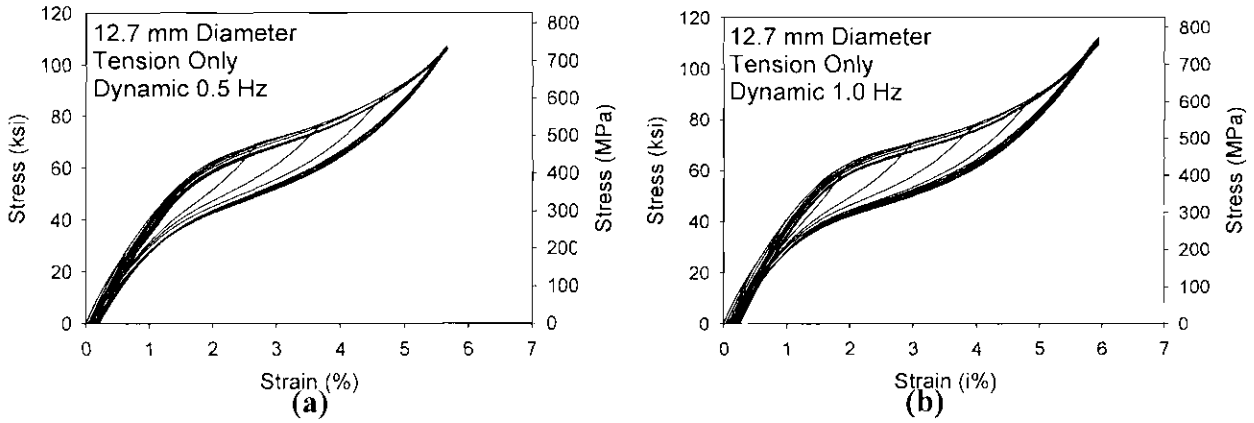

Figure 11. Stress-strain plot for the 12.7 mm (0.5 inch) diameter SE bars tested dynamically in tension at loading rates of (a) 0.5 Hz and (b) 1.0 Hz)

2.7 Conclusions

The results from the 25.4 mm (1.0 inch), 12.7 mm (0.5 inch), and 7.1 mm (0.28 inch) diameter superelastic NiTi specimens all showed good superelastic behavior under loading levels and loading rates typically experienced during an earthquake or other types of extreme loading events. For all cases the residual strain increased with increased maximum cyclic strain as expected due to the formation of permanent slip. In particular under tensile loadings, the 25.4 mm (1.0 inch) diameter bars showed slight increases in the residual strain with increased loading rate and increases in the residual strain to above 1% with continued dynamic cycling at 5% strain. Even with the increased residual strain values, the 25.4 mm diameter (1.0 inch) specimens maintained good recentering capability given the high strain level of cycling until failure. The residual strain in both of the midsize diameter bars actually decreased slightly with increased loading rate for a given strain cycle. For all tensile loadings, the midsize bars maintain good recentering capabilities with residual strains remaining below 0.75% even after four 6% strain cycles. The results suggest that midsize diameter NiTi SMAs may provide better recentering capabilities for structural applications in extreme loading events, but the possibility of using larger diameter specimens exist with further refinement of the material and processing of NiTi SMAs.

Only minimal energy dissipation capacity was obtained from all of the tensile specimens, particularly for those specimens subjected to dynamic loading rates. Dynamic loadings led to an increase in the unloading plateau in the midsize diameter specimens resulting in a pinching of the hysteresis and a loss of energy dissipation capacity. For all cases, the equivalent viscous damping remained below 4%. These equivalent viscous damping values are typically too low to suggest the use of superelastic NiTi shape memory alloys in purely damping applications for extreme loading events. Although, large diameter superelastic NiTi shape memory alloys would provide some supplemental damping to a system if they are being used as a recentering device resulting in further reduction in the response of a structure.

The results from the 25.4 mm (1.0 inch) diameter tests suggest that superelastic SMAs can be used in tension and compression bracing systems as opposed to just tension bracing systems which has been commonly suggested in the past. The compression results did show that there is a significant increase in the loading plateau stress and a significant asymmetry between the tension and compression behavior. Further, the test results suggest that for the best performance under compression loadings superelastic NiTi SMAs should be constrained from buckling. The large diameter tests also suggested that further work needs to be done in order to develop a connection system that does not promote surface defects in the material, which can result in premature failure. Overall, the tests results suggest that superelastic NiTi shape memory alloys can be used as recentering and supplemental damping devices in order to control structural response during extreme loading events, even in larger diameter forms.

3.0 Shape Memory Alloy Brace Damping Elements

3.1 Overview

Recent investigations have shown the possibility of using SMAs in applications to improve the performance of building structures undergoing seismic events. Graesser and Cozzarelli (1991) were one of the first investigators to suggest the use of binary NiTi SMAs as seismic dampers with a study of the effect of loading frequency and loading history on the energy dissipation characteristics of NiTi wires. Others have looked into the performance of actual building systems implementing SMAs. Inaudi and Kelly (1994) used a unidirectional shake table to study a four-story steel-frame model which implemented tuned mass dampers using SMA wires. More recently, investigations by Barrata and Corbi (2002) showed that the performance of structures can be modified with the use of SMA braces with their study of the dynamic performance of a portal frame. The results showed that superelastic SMA braces effectively reduced the dynamic response of the frame. Although several studies have been conducted in regards to the use of SMAs as damping element for seismic response reduction of structures, very few of these studies have looked at the performance of larger diameter specimens which would be more feasible for extreme loading structural applications.

This part of the analytical study will attempt to look at structural applications of large diameter NiTi superelastic SMAs as cross-bracing systems in a concentrically braced steel frame. Concentrically braced frames provide a solution to problems associated with steel moment resisting frames which can undergo large displacements and joint loadings. Sabelli (2001) and Sabelli et al. (2003) have found that concentric steel bracing systems can perform well during seismic events, but the use of conventional steel braces can result in yielding and permanent damage to the bracing system. The recentering capability and added damping associated with the flag-shape hysteresis of the large diameter NiTi superelastic SMAs provides a unique way to address some of these constraints of conventional steel bracing systems and an innovative way to reduce the seismic response of structures. This study will attempt to determine the viability of large diameter SE NiTi SMA braces by comparing the maximum inter-story drifts and residual displacements of the top floor of a concentrically braced steel frame with either conventional buckling allowed steel braces or superelastic shape memory alloy braces undergoing a variety of ground motions.

3.2 Analytical Model

In order to compare the seismic response of a conventional steel bracing system and a superelastic SMA bracing system, the 3-story concentrically braced steel frame presented by Sabelli (2001) is considered. Figure 1 shows the plan view and elevation view of the 3-story frame with the steel member sizes labeled along with the sizes of the conventional steel braces. Given the symmetry of the floor plan, only a single bay is considered with the appropriate story masses and loads determined based on tributary areas. For the second structure which implemented superelastic SMA braces, the same beam and column sizes were maintained. The shape memory alloys braces were designed such that the overall frame system would have the same natural period as the conventional steel braced structure. In order to obtain the same natural period, the SMA bracing system was designed to have rigid segments connecting the

specified length of the SMA brace to the frame itself as is seen in Figure 2. The use of a rigid segment ensures that all of the deformation will occur in the SMA segment of the brace. This configuration allows the stiffness of the structure to be adjusted based on the length of the SMA segment. In order to compare the effectiveness of the SMA braces to that of the conventional steel braces, the SMA braces are designed with a cross-sectional area and length so as to provide the same yield force and axial stiffness as the conventional steel braces. The geometric characteristics of the SMA segment of the innovative braces can be seen in Table 1. The performance of the two braced frames is measured based on the maximum inter-story drift and the residual drift of the top floor obtained from nonlinear time history analyses. A suite of ten LA ground motions with a 10% probability of exceedance in 50 years developed for the SAC building study is used to evaluate the structures.

Table 1. Geometric characteristics of SMA segments

Story	SMAs Braces for 3-Story Frame	
	Length mm (inch)	Area mm^2 ($inch^2$)
1	829.84 (32.67)	5259.46 (8.15)
2	829.84 (32.67)	3794.60 (5.88)
3	829.84 (32.67)	2407.66 (3.73)

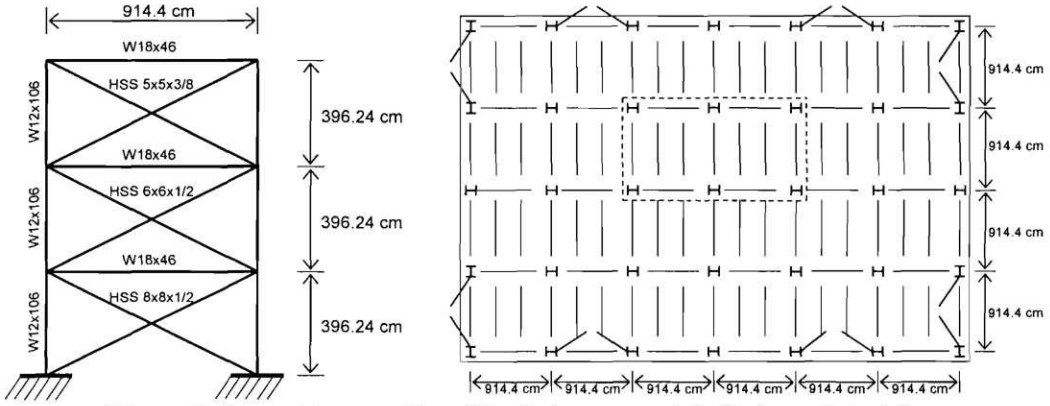

Figure 1. Geometric properties of the 3-story concentrically braced steel frame

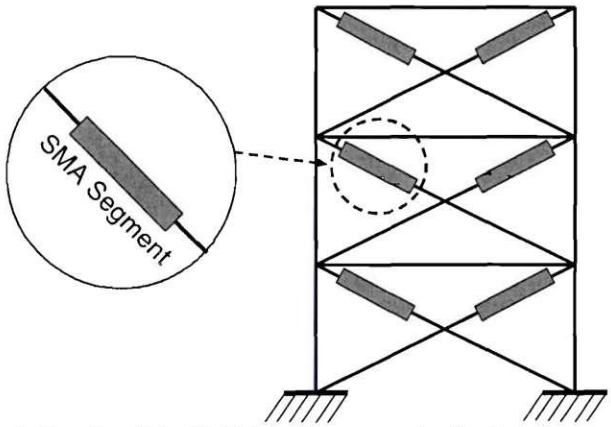

Figure 2. Details of the SMA bracing system in the 3-story steel frame

All nonlinear dynamic time history analyses are carried out using the OpenSEES platform (2003). The beam and column elements were modeled in OpenSEES using nonlinearBeamColumn elements with fiber sections. The Steel01 material is used to represent the force displacement behavior of the beams and columns. All connections are assumed to be fixed connections except for the top floor beam to column connection which is hinged. Both the conventional steel braces and the superelastic SMA braces are pinned at each end in order to ensure that they only carry axial loads. Typical Rayleigh damping of 5% for steel braced frames is considered and P-Δ effects are accounted for during the analysis.

Figure 3 provides the models for the conventional steel braces and the superelastic SMA braces. The conventional steel braces are modeled with a modified version of the hysteretic model in order to take into account the behavior of the braces after the occurrence of buckling under compression. The superelastic SMA braces are modeled as constrained from buckling in compression using a modified uniaxial constitutive model proposed by Auricchio and Sacco (1997). Assumptions are made that no strength degradation occurs with continued cycling and that the austenite and stress-induced martensite branches have the same modulus of elasticity in order to simplify the behavior. Details in regards to the continuous model and its integration techniques can be found in Fugazza (2003). The properties of the superelastic SMA braces are based on the 12.7 mm (0.5 inch) diameter midsize bar tests presented in Section 2.2 of this report.

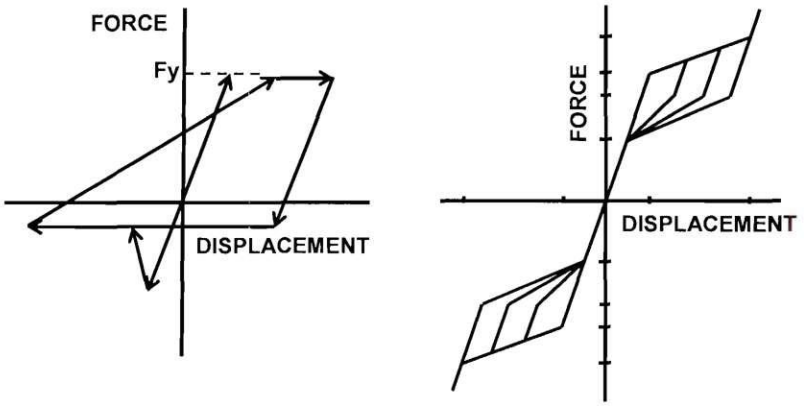

Figure 3. Force-displacement relationship for the (a) conventional steel buckling allowed braces and the (b) superelastic SMA braces

3.3 Results

In order to initially evaluate the performance of the conventional steel bracing system and the superelastic SMA bracing system, the response to the LA06 ground motion is first evaluated. The displacement time history of the upper left node for both the steel braced and SMA braced structures is shown in Figure 4. The steel braced system undergoes much higher roof displacements as compared to the superelastic SMA braced system. The maximum lateral roof displacement for the steel braced structure is approximately 480 mm (18.9 inches) as compared to approximately 99 mm (3.9 inches) for the SMA braced structure. The SMA braces reduce the maximum roof displacement by approximately 79% due to their unique flag-shape stress-strain behavior. It is also clear from the results that the recentering capability of the superelastic SMAs reduces the residual roof displacement to only 1.6 mm (0.06 inches) as compared to the residual

roof displacement obtained with the conventional steel braces of 141 mm (5.6 inches). This decreased maximum lateral roof displacement and residual roof displacement shows the optimal performance of the SE SMA braces as compared to convention buckling-allowed steel braces. The reduced values also can result in the possibility of reduced damage and minimal repairs to a structure after an extreme loading event when large diameter SE SMA braces are implemented.

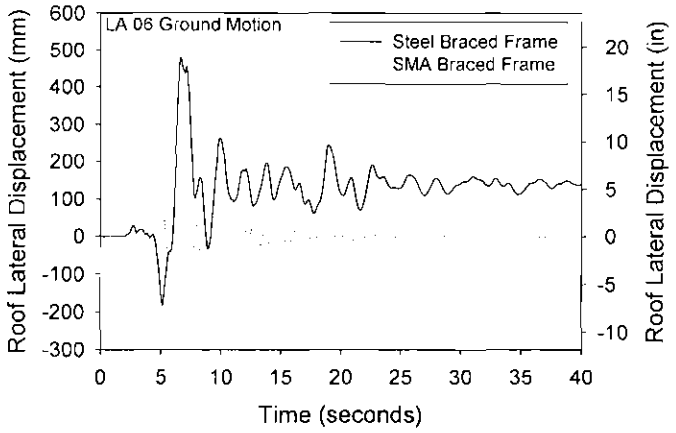

Figure 4. Roof lateral displacement time-history for the 3-story frame with either conventional steel braces or superelastic SMA braces excited by the LA06 record.

The maximum inter-story drift with respect to all ten of the ground motions is presented in Figure 5(a). The results show further evidence that midsize and large diameter NiTi SMA bracing systems can limit maximum inter-story drift as compared to conventional steel bracing systems. In all cases, the steel braced structure had significantly higher values of maximum inter-story drift as compared to the SMA braced structure with the largest inter-story drift for the SE SMA braced structure only reaching 1.03%. In contrast, the smallest maximum inter-story drift associated with the conventional steel braced structure came as a result of the LA02 ground motion and was approximately 1.3%. On average, the superelastic SMA braces reduced the maximum inter-story drift by 69% with respect to the maximum inter-story drift values obtained when conventional steel braces were used. The better performance of the SE SMA braced structures can be attributed to the recentering capability of the superelastic SMAs which limits the accumulation of permanent deformation in the bracing members.

The residual drift of the top floor for all of the ground motions is shown in Figure 5(b) and provides further evidence of the ability of large diameter superelastic SMAs to reduce the structural response of building structures and prevent permanent damage. The maximum residual drift values for the conventional steel braced structure is over 90 times larger than the maximum residual drift associated with the SMA braced structure where the maximum drifts are 1.19% and 0.013% for the steel braced and SMA braced structures, respectively. In no case did the residual top floor drift for the SMA braced frame surpass the minimum residual drift of the conventional steel braced frame. The larger residual drifts in the conventional steel braced frame can be attributed to permanent yielding and buckling of the steel braces when a number of large displacement cycles occurred causing a reduction in their effectiveness. Overall, the innovative superelastic SMA bracing system proved to reduce structural response more effectively through

a combination of both recentering capability and supplemental damping due to the unique flag-shape hysteretic behavior.

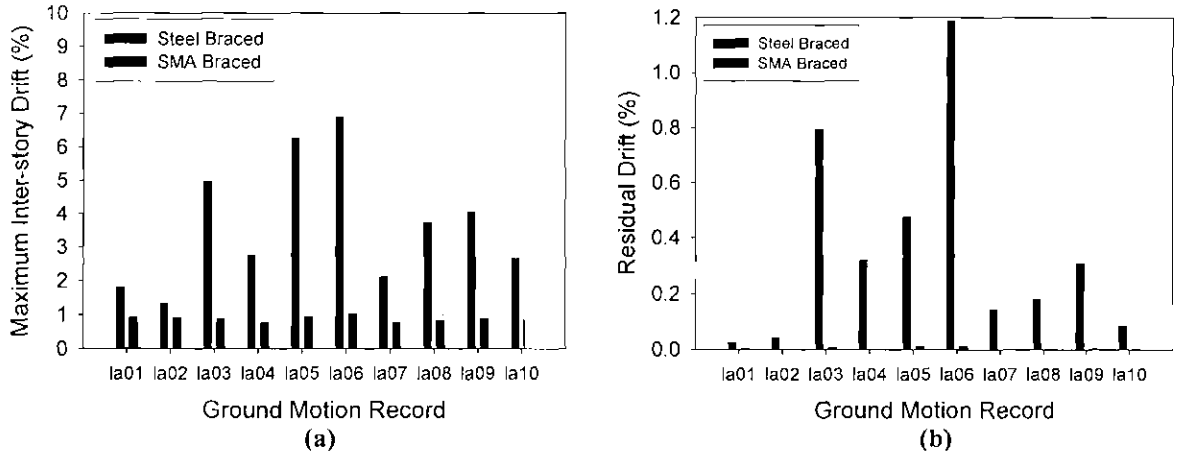

Figure 5. (a) Maximum inter-story drift and (b) residual drift of the top floor exhibited by the 3-story concentrically braced steel frame with either conventional steel braces or superelastic SMA braces

3.4 Conclusions

The analytical comparison of a concentrically braced steel frame with either conventional buckling allowed steel braces or midsize diameter superelastic SMA braces showed the effectiveness of SMA bracing systems in reducing the response of structures under extreme loadings. The superelastic effect is clearly effective in reducing the maximum inter-story drift and residual drift of the top story. Since the steel braces produce hysteresis loops with a significantly larger area as compared to those produced by the SMA braces, the ability of the SMAs to recover their undeformed shape and provide recentering to the system must be one of the main contributing factors to the reduced dynamic response of the SMA braced structure. The results suggest promise in the future use of large diameter superelastic SMAs in bracing systems, although continued work is necessary in order to determine optimal bracing configurations and whether reduced cross-sectional area of SMAs can provide similar results while also reducing the cost of such systems.

References

Auricchio, F., and Sacco, E., 1997, "A One-Dimensional Model for Superelastic Shape-Memory Alloys with Different Properties Between Martensite and Austenite," *International Journal of Non-Linear Mechanics*, **32**, pp. 1101-1114.

Baratta, A., and Corbi, O., 2002, "On the Dynamic Behaviour of Elastic-Plastic Structures Equipped with Pseudoelastic SMA Reinforcements," *Computational Materials Science*, **25**, pp. 1-13.

Fugazza, D., 2003, "Shape-Memory Alloy Devices for Earthquake Engineering: Mechanical Properties, Constitutive Modeling and Numerical Simulations," *Masters' Thesis*, European School for Advanced Studies in Reduction of Seismic Risk, Pavia, Italy.

Graesser, E. J., and F. A. Cozzarelli, 1991, "Shape-Memory Alloys As New Materials for Aseismic Isolation." *Journal of Engineering Mechanics*, **117**,11, pp. 2590-608.

Inaudi, J., and Kelly, J., 1994, "Experiments on Tuned Mass Dampers Using Viscoelastic, Frictional and Shape-Memory Alloy Materials." *First World Conference on Structural Control*, Los Angeles, CA, pp. 127-136.

Sabelli, R., 2001, "Research on Improving the Design and Analysis of Earthquake-Resistant Steel-Braced Frames," *Professional Fellowship Report* No. PF2000-9, NEHRP, USA.

Sabelli, R., Mahin, S., Chang, C., 2003, "Seismic Demands on Steel Braced Frame Buildings with Buckling-Restrained Braces," *Engineering Structures*, **25**, pp. 655-666.